In conclusion, our data suggest that reduction of GIP secretion *in vivo* confirms the potent role of GIP in insulin secretion and leads to reduced obesity and reduced insulin resistance in high fat diet conditions without severely impairing glucose homeostasis and without disrupting the role of GIP in bone formation. These findings are potentially promising of a new therapeutic approach to obesity and type 2 diabetes mellitus.

Acknowledgements

The authors thank Mr. Shoichi Asano and Dr. Xibao Liu from the Department of Diabetes, Endocrinology and Nutrition, Graduate School of Medicine, Kyoto University, for their technical support regarding the study. This study was supported by Scientific Research Grants from the Ministry of Education, Culture, Sports, Science, and Technology, Japan, and from the Ministry of Health, Labor, and Welfare, Japan.

D.N., N.H., K.Su., S.Y., A.H., E.J., K.I., K.Sh., and T.H. have no conflict of interest to disclose. N.I. served as a medical advisor for Takeda, Taisho Pharmaceutical, GlaxoSmithKline, Mitsubishi Tanabe Pharma, he lectured for MSD, Sanofi, Novartis Pharma, Dainippon Sumitomo Pharma, Kyowa Kirin, and Mitsubishi Tanabe Pharma, and received payment for his services. N.I. also received a clinical commissioned/joint research grant from MSD, Eli Lilly Japan, Shiratori Pharmaceutical, Roche Diagnostics, and the Japan Diabetes Foundation, and also received a scholarship grant from MSD, JT, Nippon Boehringer Ingelheim, Takeda, Dainippon Sumitomo Pharma, Astellas Pharma, Daiichi-Sankyo, and Mitsubishi Tanabe Pharma.

D.N. researched the data, contributed to discussion, wrote, reviewed and edited the manuscript. N.H. contributed to discussion, reviewed and edited the manuscript. K.Su., S.Y., A.H., E.J., K.I., K.Sh., and T.H. contributed to discussion. N.I contributed to discussion, reviewed and edited the manuscript.

N.I. is the guarantor of this work and, as such, had full access to all the data in the study and takes responsibility for the integrity of the data and the accuracy of the data analysis.

Parts of the study were presented in an abstract form at the 47th Annual Meeting of the European Association for the study of Diabetes in Lisbon, Portugal, 12-16 September 2011, at the 48th Annual Meeting of the European Association for the study of Diabetes in Berlin, Germany, 1-5 October 2012, and at the 73rd Scientific Sessions of the American Diabetes Association in Chicago, Illinois, 21-25 June 2013.

References:

1. Krarup T, Holst JJ, Lindorf Larsen K. Responses and molecular heterogeneity of IR-GIP after intraduodenal glucose and fat. Am J Physiol. 1985; 249 (2 Pt 1): E195-E200.
2. Flatt PR. Dorothy Hodgkin Lecture 2008 Gastric inhibitory polypeptide (GIP) revisited: a new therapeutic target for obesity–diabetes? Diabetic Med. 2008; 25 (7): 759-764.
3. Baggio LL, Drucker DJ. Biology of incretins: GLP-1 and GIP. Gastroenterology. 2007; 132 (6): 2131-2157.
4. Pederson RA, Brown JC. Inhibition of histamine-, pentagastrin-, and insulin-stimulated canine gastric secretion by pure "gastric inhibitory polypeptide". Gastroenterology. 1972; 62 (3): 393-400.
5. Dupre J, Ross SA, Watson D, Brown JC. Stimulation of insulin secretion by gastric inhibitory polypeptide in man. J Clin Endocrinol Metab. 1973; 37 (5): 826-828.
6. Yamada Y, Miyawaki K,Tsukiyama K, Harada N, Yamada C, Seino Y. Pancreatic and extrapancreatic effects of gastric inhibitory polypeptide. Diabetes. 2006; 55, Supplement 2, S86-S91.
7. Miyawaki K, Yamada Y, Yano H et al. Glucose intolerance caused by a defect in the entero-insular axis: A study in gastric inhibitory polypeptide receptor knockout mice. P Natl Acad Sci USA. 1999; 96 (26): 14843-14847.
8. Herbach N, Bergmayr M, Göke B, Wolf E, Wanke R. Postnatal development of numbers and mean sizes of pancreatic islets and beta-cells in healthy mice and GIPR^{dn} transgenic diabetic mice. PLos ONE. 2011; 6 (7): e22814.
9. Renner S, Fehlings C, Herbach N et al. Glucose intolerance and reduced proliferation of pancreatic β-cells in transgenic pigs with impaired glucose-dependent insulinotropic peptide function. Diabetes. 2010; 59 (5): 1228-1238.
10. Kim SJ, Winter K, Nian C, Tsuneoka M, Koda Y, McIntosh CH. Glucose-dependent insulinotropic polypeptide (GIP) stimulation of pancreatic β-cell survival is dependent upon phosphatidylinositol 4-kinase (PI3K)/protein kinase B (PKB) signaling, inactivation of the forkhead transcription factor Foxo1, and downregulation of bax expression. J Biol Chem. 2005; 280 (23): 22297-22307.

11. Widenmaier SB, Kim SJ, Yang GK et al. A GIP receptor agonist exhibits β-cell anti-apoptotic actions in rat models of diabetes resulting in improved β-cell function and glycemic control. PLoS One. 2010; 5 (3): e9590.
12. Miyawaki K, Yamada Y, Ban N et al. Inhibition of gastric inhibitory polypeptide signaling prevents obesity. Nat Med. 2002; 8 (7): 738-742.
13. Tsukiyama K, Yamada Y, Yamada C et al. Gastric inhibitory polypeptide as an endogenous factor promoting new bone formation after food ingestion. Mol Endocrinol. 2006; 20 (7): 1644-1651.
14. McClean PL, Irwin N, Cassidy RS, Holst JJ, Gault VA, Flatt PR. GIP receptor antagonism reverses obesity, insulin resistance, and associated metabolic disturbances induced in mice by prolonged consumption of high-fat diet. Am J Physiol Endocrinol Metab. 2007; 293 (6): E1746-E1755.
15. Suzuki K, Harada N, Yamane S et al. Transcriptional regulatory factor X6 (Rfx6) increases gastric inhibitory polypeptide (GIP) expression in enteroendocrine K-cells and is involved in GIP hypersecretion in high fat diet-induced obesity. J Biol Chem. 2013; 288 (3): 1929-1938.
16. Preitner F, Ibberson M, Franklin I et al. Gluco-incretins control insulin secretion at multiple levels as revealed in mice lacking GLP-1 and GIP receptors. J Clin Invest. 2004; 113 (4): 635-645.
17. Yamane S, Harada N, Hamasaki A et al. Effects of glucose and meal ingestion on incretin secretion in Japanese subjects with normal glucose tolerance. J Diabetes Invest. 2012; 3 (1) 80-85.
18. Vollmer K, Holst JJ, Baller B et al. Predictors of incretin concentrations in subjects with normal, impaired, and diabetic glucose tolerance. Diabetes. 2008; 57 (3): 678-687.
19. Althage MC, Ford EL, Wang S, Tso P, Polonsky KS, Wice BM. Targeted ablation of glucose-dependent insulinotropic polypeptide-producing cells in transgenic mice reduces obesity and insulin resistance induced by high fat diet. J Biol Chem. 2008; 283 (26): 18365-18376.
20. Fujita Y, Chui JWY, King DS et al. Pax6 and Pdx1 are required for production of glucose-dependent insulinotropic polypeptide in proglucagon-expressing L cells. Am J Physiol Endocrinol Metab. 2008; 295 (3): E648-E657.
21. Parker HE, Habib AM, Rogers GJ, Gribble F, Reimann F. Nutrient-dependent secretion of glucose-dependent insulinotropic polypeptide from primary murine K cells. Diabetologia. 2009; 52 (2): 289-298.
22. Habib AM, Richards P, Cairns LS et al. Overlap of endocrine hormone expression in the mouse intestine revealed by transcriptional profiling and flow cytometry. Endocrinology. 2012; 153 (7): 3054-3065.
23. Brubaker PL. Regulation of intestinal proglucagon-derived peptide secretion by intestinal regulatory peptides. Endocronology. 1991; 128 (6): 3175-3182.
24. Roberge JN, Brubaker PL. Regulation of proglucagon-derived peptide secretion by glucose-dependent insulinotropic peptide in a novel enteroendocrine loop. Endocrinology. 1992; 133 (1): 233-240.
25. Pacheco-Pantoja EL, Ranganath LR, Gallager JA, Wilson PJM, Fraser WD. Receptors and effects of gut hormones in three osteoblastic cell lines. BMC Physiol. 2011; 11:12 1-14.

26. Zhong Q, Itokawa T, Sridhar S et al. Effects of glucose-dependent insulinotropic peptide on osteoclast function. Am J Physiol Endocrinol Metab. 2007; 292 (2): E543-E548.
27. Kieffer TJ. GIP or not GIP? That is the question. Trends Pharmacol Sci 2003; 24(3):110-2.
28. Creutzfeldt W, Ebert R, Willms B et al. Gastric inhibitory polypeptide (GIP) and insulin in obesity: increased response to stimulation and defective feedback control of serum levels. Diabetologia. 1978; 14 (1): 15-24.
29. Hansotia T, Maida A, Flock G et al. Extrapancreatic incretin receptors modulate glucose homeostasis, body weight, and energy expenditure. J Clin Invest. 2007; 117 (1): 143-152.
30. Harada N, Yamada Y, Tsukiyama K et al. A novel GIP receptor splice variant influences GIP sensitivity of pancreatic beta-cells in obese mice. Am J Physiol Endocrinol Metab. 2008; 294 (1): E61-E68.
31. Harada N, Hamasaki A, Yamane S et al. Plasma gastric inhibitory polypeptide and glucagon-like peptide-1 levels after glucose loading are associated with different factors in Japanese subjects. J Diabetes Invest. 2011; 2 (3): 193-199.
32. Seino Y, Yabe D. Glucose-dependent insulinotropic polypeptide and glucagon-like peptide-1: Incretin actions beyond the pancreas. J Diabetes Invest. 2013; 4 (2): 108-130.
33. Knapper JME, Puddicombe SM, Morgan LM, Fletcher JM. Investigations into the actions of glucose-dependent insulinotropic polypeptide and glucagon-like peptide-1 (7-36) on lipoprotein lipase activity in explants of rat adipose tissue. J Nutr. 1995; 125: 183-188.
34. Song DH, Getty-Kaushik L, Tseng E, Simon J, Corkey BE, Wolfe MM. Glucose-dependent insulinotropic polypeptide enhances adipocytes development and glucose uptake in part through Akt activation. Gastroenterology. 2007; 133 (6): 1796-1805.
35. Parkin SM, Walker K, Ashby P, Robinson DS. Effects of glucose and insulin on the activation of lipoprotein lipase and on protein synthesis in rat adipose tissue. Biochem J. 1980; 188 (1): 193-199.
36. Mehran AE, Templeman NM, Brigidi GS et al. Hyperinsulinemia drives diet-induced obesity independently of brain insulin production. Cell Metab 2012; 16(6):723-37.
37. Naitoh R, Miyawaki K, Harada N et al. Inhibition of GIP signaling modulates adiponectin levels under high-fat diet in mice. Biochem Biophys Res Commun. 2008; 376 (1): 21-25.
38. Zhou H, Yamada Y, Tsukiyama K et al. Gastric inhibitory polypeptide modulates adiposity and fat oxidation under diminished insulin action. Biochem Biophys Res Commun. 2005; 335 (3): 937-942.
39. Faivre E, Gault VA, Thorens B, Hölscher C. Glucose-dependent insulinotropic polypeptide receptor knockout mice are impaired in learning, synaptic plasticity and neurogenesis. J Neurophysiol. 2011; 105 (4): 1574-1580.
40. Yamada C, Yamada Y, Tsukiyama K et al. Genetic inactivation of GIP signaling reverses aging-associated insulin resistance through body composition changes. Biochem Biophys Res Commun. 2007; 364 (1): 175-180.

Figure legends:

Figure 1. GIP reduction in GIP-GFP KI mice. Following measurements were conducted in small intestine of WT, $GIP^{gfp/+}$ and $GIP^{gfp/gfp}$ mice: assessment of GIP mRNA levels (expressed as GIPR mRNA/GAPDH mRNA) and GIP content (expressed as GIP/protein content) (A). Total GIP levels (B) and GIP secretion (AUC-GIP) (C) were measured during OGTT (glucose 2g/kg of body weight). n=5-6 per group. WT mice are represented by white bars and white circles, $GIP^{gfp/+}$ mice by black bars and black squares, and $GIP^{gfp/gfp}$ mice by gray bars and gray triangles. *p<0.05, **p<0.01, ***p<0.001.

Figure 2. Body weight, glucose tolerance and β-cell profile following GIP reduction in standard chow-fed mice

Body weight (A) of weaning mice (4 weeks-old) was measured starting from the beginning of the weaning period until the age of 8 weeks (body weight in the 7^{th} week of age was not measured due to CT scan measurement and post-anesthesia recovery period). Body fat (B) was measured by CT scan in the 7^{th} week of age. Glucose (C) and insulin levels (D) were measured during OGTT (glucose load of 2g/kg of body weight). *In vitro* insulin secretion from isolated islets (E) was measured in conditions of 5.5 mM glucose, 11.1 mM glucose, and 11.1 mM glucose + 100 nM human GIP peptide. GIP receptor mRNA levels in islets (F) were expressed as GIPR mRNA/GAPDH mRNA. n= 5-6 mice or samples per group; 10 islets per sample. WT mice are represented by white circles and white bars, $GIP^{gfp/+}$ mice by black squares and black bars, and $GIP^{gfp/gfp}$ mice by gray triangles and gray bars. *p<0.05, **p<0.01 vs. WT; $^{\#}$p<0.05 vs. $GIP^{gfp/+}$ mice.

Figure 3. Bone formation in conditions of standard chow feeding. Following parameters were measured by bone histomorphometry: bone volume (expressed as bone volume %) (A),

trabeculae number (expressed as number/mm) (C), osteoblast surface (%) (D), osteoclast surface (%) (E), and bone formation rate (%/year) (F). Images display trabeculae of proximal tibial sections (B) taken from 6 weeks-old mice. n=5-6 per group. WT mice are represented by white bars, $GIP^{gfp/+}$ mice by black bars, and $GIP^{gfp/gfp}$ mice by gray bars. *p<0.05 vs. WT. Absence of asterisk above the horizontal brackets in Fig. 3A, 3C, 3D and 3E indicates no statistical significance.

Figure 4. Induction of metabolic stress by HFD. Body weight (A) and ad libitum glucose levels (B) in WT CFD, WT HFD, $GIP^{gfp/+}$ HFD and $GIP^{gfp/gfp}$ HFD mice were measured once per week during 8 weeks (56 days) of CFD (10% of fat) or HFD (60% of fat). Total GIP levels (C), GIP secretion (GIP-AUC) (D), glucose levels (E), and insulin levels (F) were measured during OGTT (glucose load of 1g/kg of body weight) conducted after 8 weeks (56 days) of CFD or HFD. *In vitro* insulin secretion from isolated islets (G) was measured in conditions of 5.5 mM glucose, 11.1 mM glucose and 11.1 mM glucose + 100 nM human GIP peptide. Results were expressed as insulin secretion (% insulin content). β-cell area (H) was measured by immunohistochemistry of pancreas sections and subsequent analysis using BZ Analyzer software. Results are expressed as β-cell area/total pancreas area. GIP receptor mRNA levels in islets (I) were expressed as GIPR mRNA/GAPDH mRNA. n= 5-6 mice or samples per group; 10 islets per sample. WT CFD mice are represented by white circles with square dot dash and white bars with square dot border, WT HFD mice by white circles with solid dash and white bars with solid border, $GIP^{gfp/+}$ mice by black squares and black bars, and $GIP^{gfp/gfp}$ mice by gray triangles and gray bars. P values are expressed as follows: Fig.4A, 4C, 4D, 4E, 4F:*p<0.05, **p<0.01, ***p<0.001 vs. WT HFD. Fig.4B: *p<0.05 WT CFD vs. WT HFD and $^{\#}$p<0.05 $GIP^{gfp/+}$ HFD vs.

WT HFD. Fig.4G, 4H and 4I:*p<0.05, **p<0.01, ***p<0.001. Absence of asterisk above the horizontal brackets in Fig. 4G, 4H and 4I indicates no statistical significance.

Figure 5. Adipose tissue response to HFD feeding and consequential energy expenditure changes. Visceral, subcutaneous and total fat (expressed in g) in WT CFD, WT HFD, $GIP^{gfp/+}$HFD and $GIP^{gfp/gfp}$ HFD mice (A) were measured, and CT images of transversal abdominal sections were taken after 8 weeks of CFD (10% of fat) or HFD (60% of fat). ITT (insulin 0.5 U/kg of body weight) was conducted after 8 weeks of CFD or HFD (B). Fat oxidation (mg/min/kg) (C), energy expenditure (cal/min/kg) (D) and mice activity (counts/min) (E) were measured after 6-7 weeks of CFD or HFD. GIP receptor mRNA levels in white (visceral) adipose tissue (F) were expressed as GIPR mRNA/GAPDH mRNA. n= 5-6 mice or samples per group. WT CFD mice are represented by white bars with square dot border and white circles with square dot dash, WT HFD mice by white bars with solid border and white circles with solid dash, $GIP^{gfp/+}$ HFD mice by black bars and black squares, and $GIP^{gfp/gfp}$ HFD mice by gray bars and gray triangles. P values are expressed as follows: Fig.5B *p<0.05, **p<0.01, ***p<0.001 vs. WT HFD; Fig. 5A, 5C, 5D, and 5F *p<0.05, **p<0.01. Absence of asterisk above the horizontal brackets in Fig. 5A, 5C, 5D, and 5F indicates no statistical significance.

Supplementary figure 1. Body weight progression and insulin sensitivity in standard chow-fed mice. Body weight (A) of WT, $GIP^{gfp/+}$, and $GIP^{gfp/gfp}$ mice on CFD was measured once per week during 8 weeks (56 days), starting from 7 weeks of age. ITT (insulin 0.5 U/kg of body weight) was conducted after 8 weeks of standard diet feeding (B). n=5-6 mice per group. WT mice are represented by white circles with solid dash, $GIP^{gfp/+}$ mice by black squares, and $GIP^{gfp/gfp}$ mice by gray triangles. *p<0.05 $GIP^{gfp/gfp}$ vs WT.

Table 1

Phenotype comparison of GIP-GFP KI mice and GIPRKO mice

Genotype/ Phenotype	**WT**	**GIP$^{gfp/+}$**	**GIP$^{gfp/gfp}$**	**GIPRKO[7,13]**
Standard chow feeding				
GIP secretion		↓ (~50%)	absent	↑
Glucose tolerance		impaired	impaired	impaired
Bone volume		↔	↓	↓
High fat diet feeding				
	WT HFD	**GIP$^{gfp/+}$ HFD**	**GIP$^{gfp/gfp}$ HFD**	**GIPRKO HFD[6,12,29]**
Glucose tolerance		↔	↔	impaired
Body weight		↓	↓↓	↓↓
Fat mass		↓	↓↓	↓↓
Insulin sensitivity		↑	↑↑	↑↑

Standard chow feeding data are relative to WT; high fat diet feeding data are relative to WT HFD.

Symbols: "↔": no changes; "↓": decreased; "↓↓": highly decreased; "↑": increased; "↑↑": highly increased. Numbers shown in superscript indicate the corresponding articles listed in *References*.

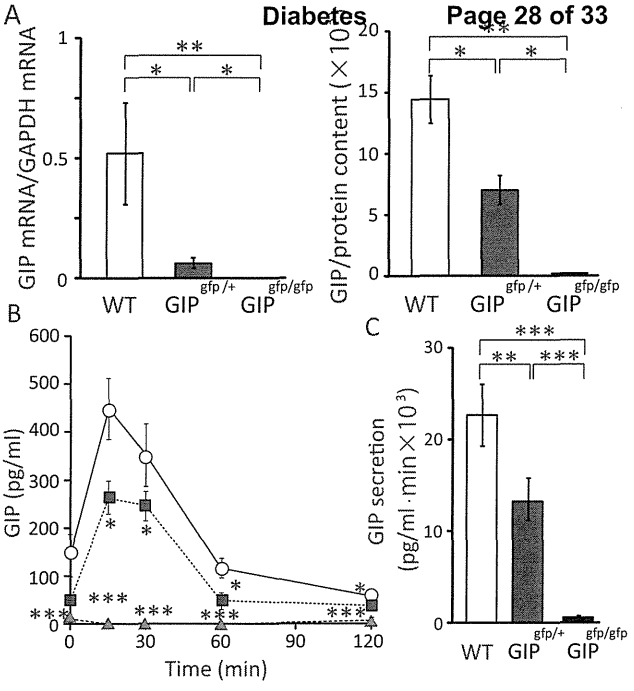
A
GIP mRNA/GAPDH mRNA
1
0.5
0
**
*
*
WT
GIP gfp/+
GIP gfp/gfp
GIP/protein content (×10
20
15
10
5
0
B
GIP (pg/ml)
600
500
400
300
200
100
0
Time (min)
0
30
60
90
120
C
GIP secretion (pg/ml·min×10³)
30
20
10
0
***
**

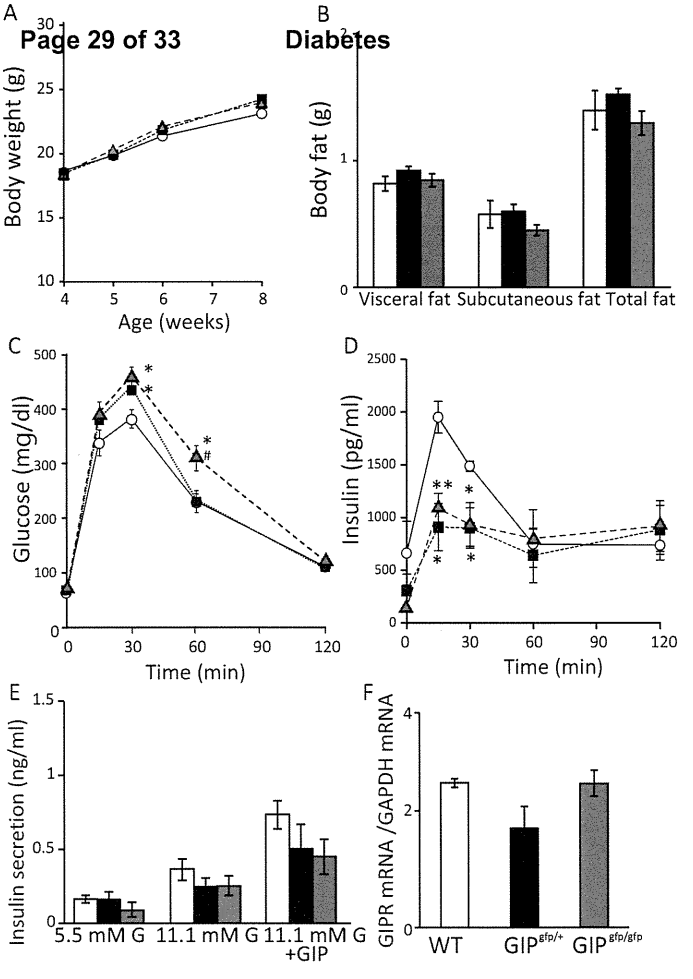
A
Body weight (g)
Age (weeks)
B
Body fat (g)
Visceral fat
Subcutaneous fat
Total fat
C
Glucose (mg/dl)
Time (min)
D
Insulin (pg/ml)
Time (min)
E
Insulin secretion (ng/ml)
5.5 mM G
11.1 mM G
11.1 mM G +GIP
F
GIPR mRNA /GAPDH mRNA
WT
GIP gfp/+
GIP gfp/gfp

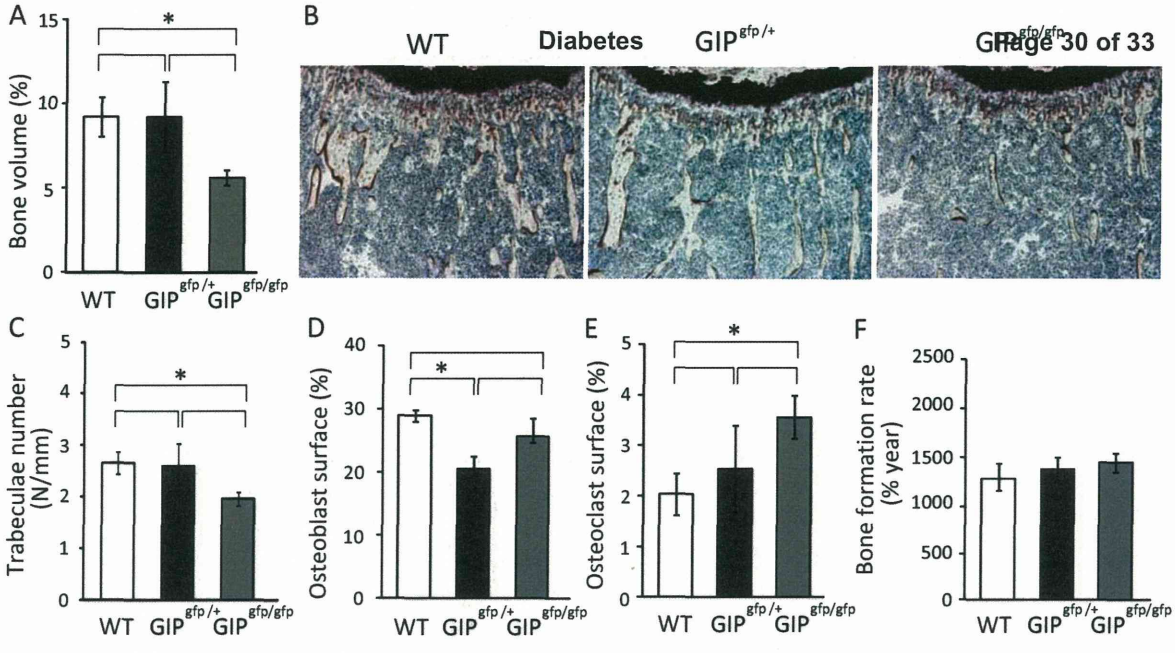
A
Bone volume (%)
15
10
5
0
*
WT
GIP gfp/+
GIP gfp/gfp
B
WT
Diabetes
GIP gfp/+
GIP gfp/gfp
C
Trabeculae number (N/mm)
5
4
3
2
1
0
*
WT
GIP gfp/+
GIP gfp/gfp
D
Osteoblast surface (%)
40
30
20
10
0
*
WT
GIP gfp/+
GIP gfp/gfp
E
Osteoclast surface (%)
5
4
3
2
1
0
*
WT
GIP gfp/+
GIP gfp/gfp
F
Bone formation rate (% year)
2500
2000
1500
1000
500
0
WT
GIP gfp/+
GIP gfp/gfp

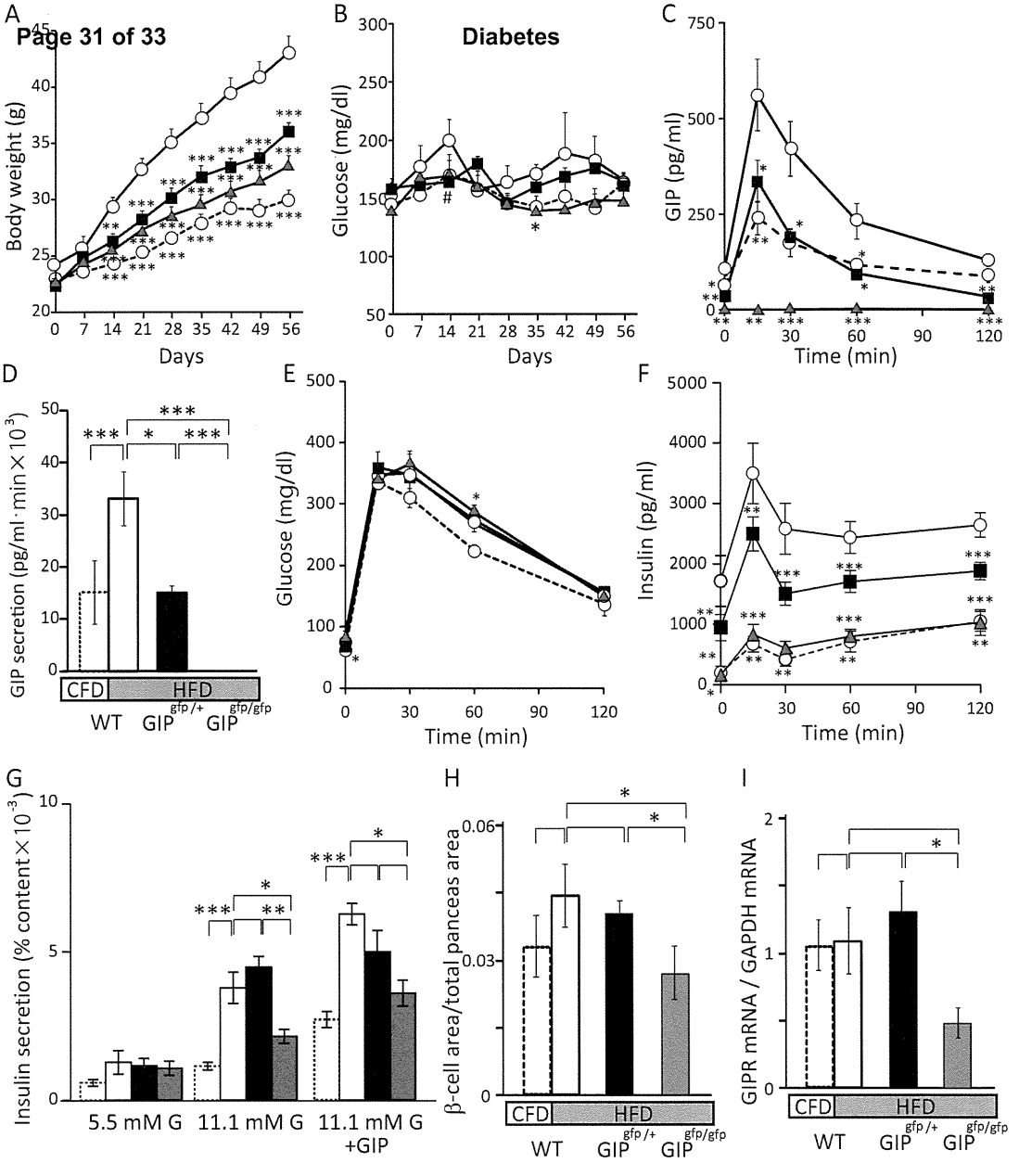
A
Body weight (g)
Days
B
Diabetes
Glucose (mg/dl)
Days
C
GIP (pg/ml)
Time (min)
D
GIP secretion (pg/ml·min×10³)
CFD
HFD
WT
GIP gfp/+
GIP gfp/gfp
E
Glucose (mg/dl)
Time (min)
F
Insulin (pg/ml)
Time (min)
G
Insulin secretion (% content×10⁻³)
5.5 mM G
11.1 mM G
11.1 mM G +GIP
H
β-cell area/total panceas area
CFD
HFD
WT
GIP gfp/+
GIP gfp/gfp
I
GIPR mRNA / GAPDH mRNA
CFD
HFD
WT
GIP gfp/+
GIP gfp/gfp

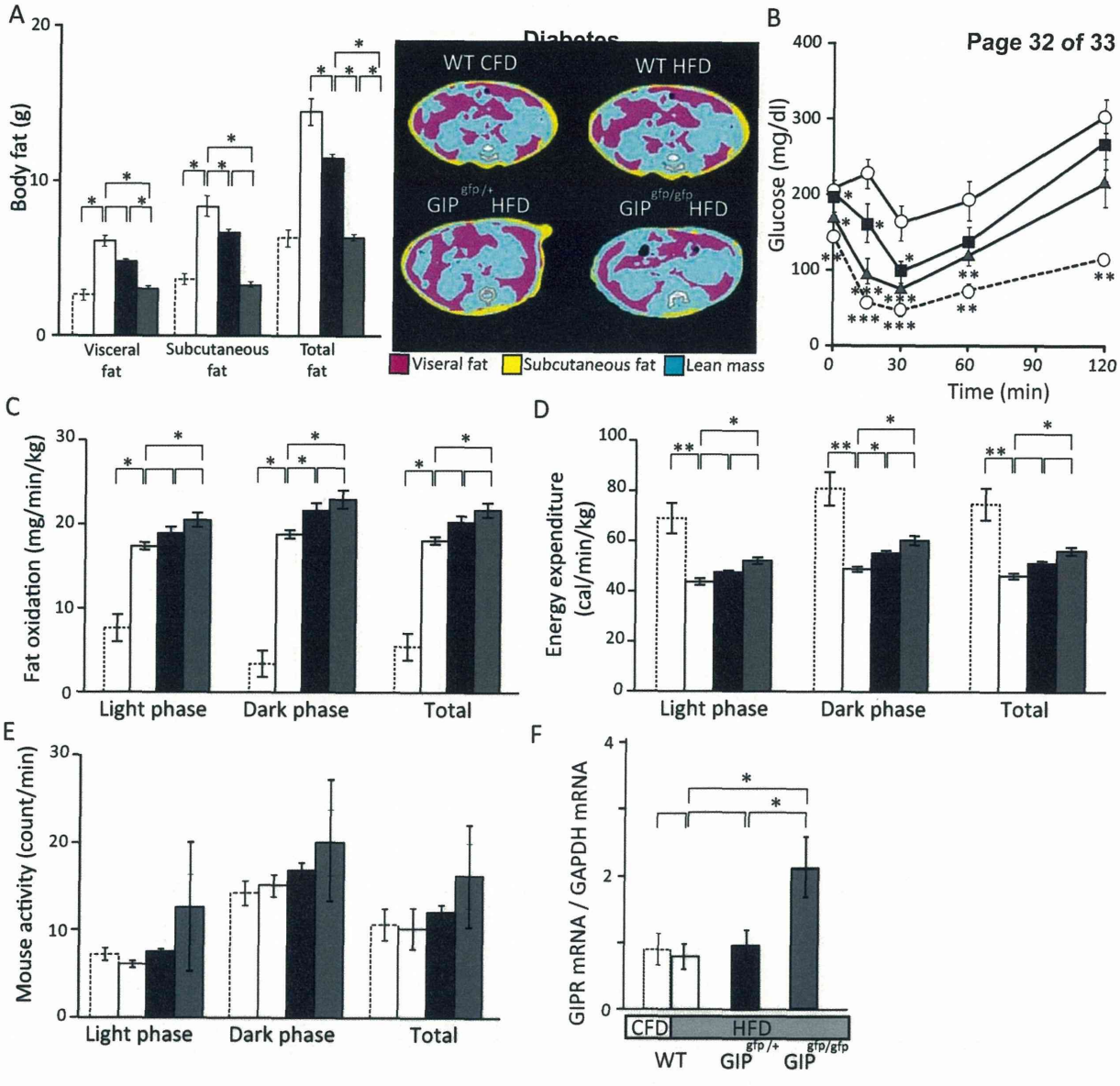
A
Body fat (g)
Visceral fat
Subcutaneous fat
Total fat
WT CFD
WT HFD
GIP gfp/+ HFD
GIP gfp/gfp HFD
Viseral fat
Subcutaneous fat
Lean mass
B
Glucose (mg/dl)
Time (min)
C
Fat oxidation (mg/min/kg)
Light phase
Dark phase
Total
D
Energy expenditure (cal/min/kg)
Light phase
Dark phase
Total
E
Mouse activity (count/min)
Light phase
Dark phase
Total
F
GIPR mRNA / GAPDH mRNA
CFD
HFD
WT
GIP gfp/+
GIP gfp/gfp

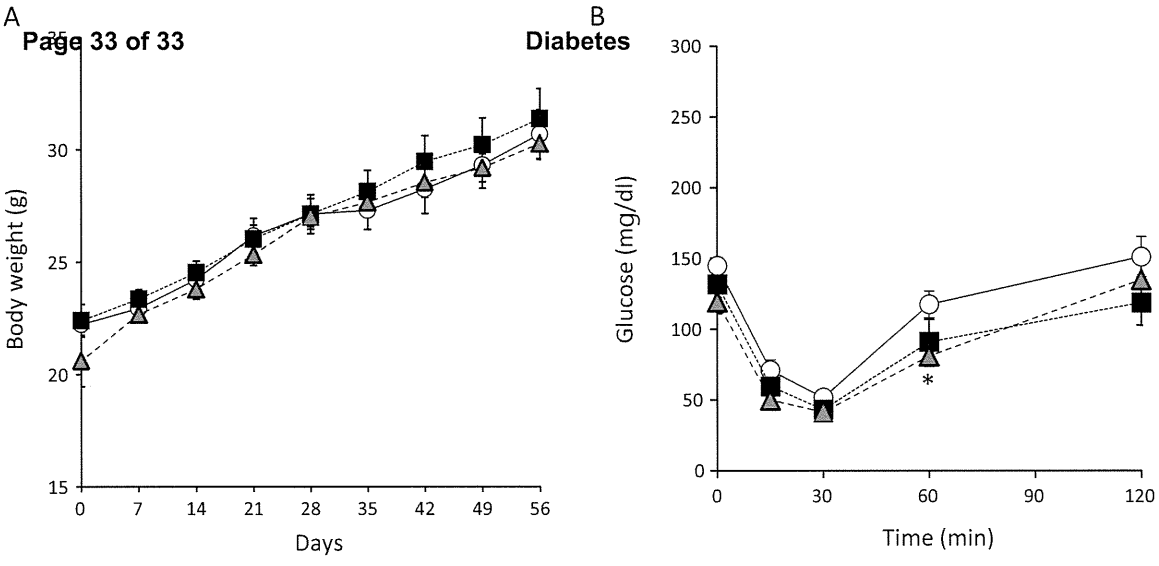
A
Body weight (g)
Days
B
Diabetes
Glucose (mg/dl)
Time (min)
*

Published April 21, 2014

BARP suppresses voltage-gated calcium channel activity and Ca^{2+}-evoked exocytosis

Pascal Béguin,[1,5] Kazuaki Nagashima,[3] Ramasubbu N. Mahalakshmi,[1] Réjan Vigot,[5] Atsuko Matsunaga,[5] Takafumi Miki,[4] Mei Yong Ng,[1] Yu Jin Alvin Ng,[1] Chiaw Hwee Lim,[1] Hock Soon Tay,[2] Le-Ann Hwang,[2] Dmitri Firsov,[6] Bor Luen Tang,[7] Nobuya Inagaki,[3] Yasuo Mori,[4] Susumu Seino,[9] Thomas Launey,[5] and Walter Hunziker[1,8]

[1]Epithelial Cell Biology Laboratory and [2]Monoclonal Antibody Unit, Institute of Molecular and Cell Biology, Agency for Science, Technology and Research, Singapore 138673
[3]Department of Diabetes and Clinical Nutrition, Graduate School of Medicine; and [4]Department of Synthetic Chemistry and Biological Chemistry, Graduate School of Engineering; Kyoto University, Sakyo-ku, Kyoto 606-8501, Japan
[5]Launey Research Unit for Molecular Neurocybernetics, RIKEN Brain Science Institute, Wako-shi, Saitama 351-0198, Japan
[6]Pharmacology and Toxicology Department, University of Lausanne, 1005 Lausanne, Switzerland
[7]Department of Biochemistry and [8]Department of Physiology, Yong Loo Lin School of Medicine, National University of Singapore, Singapore 117599
[9]Division of Cellular and Molecular Medicine, Kobe University Graduate School of Medicine, Chuo-ku, Kobe 650-0047, Japan

Voltage-gated calcium channels (VGCCs) are key regulators of cell signaling and Ca^{2+}-dependent release of neurotransmitters and hormones. Understanding the mechanisms that inactivate VGCCs to prevent intracellular Ca^{2+} overload and govern their specific subcellular localization is of critical importance. We report the identification and functional characterization of VGCC β-anchoring and -regulatory protein (BARP), a previously uncharacterized integral membrane glycoprotein expressed in neuroendocrine cells and neurons. BARP interacts via two cytosolic domains (I and II) with all $Ca_v\beta$ subunit isoforms, affecting their subcellular localization and suppressing VGCC activity. Domain I interacts at the α_1 interaction domain–binding pocket in $Ca_v\beta$ and interferes with the association between $Ca_v\beta$ and $Ca_v\alpha1$. In the absence of domain I binding, BARP can form a ternary complex with $Ca_v\alpha1$ and $Ca_v\beta$ via domain II. BARP does not affect cell surface expression of $Ca_v\alpha1$ but inhibits Ca^{2+} channel activity at the plasma membrane, resulting in the inhibition of Ca^{2+}-evoked exocytosis. Thus, BARP can modulate the localization of $Ca_v\beta$ and its association with the $Ca_v\alpha1$ subunit to negatively regulate VGCC activity.

Introduction

Exocytosis in response to action potential–evoked membrane depolarization has been extensively characterized in the nervous system, in which neurotransmitters or hormones are released after extracellular Ca^{2+} influx at synapses in neurons or in neuroendocrine cells, respectively. In pancreatic islet β cells, for example, glucose elevation results in the closure of K_{ATP} channels, membrane depolarization, opening of voltage-gated calcium channels (VGCCs), and, in response to Ca^{2+} influx, secretion of insulin (Yang and Berggren, 2006). At neuronal synapses, neurotransmitter-containing vesicles are docked in close vicinity to VGCCs at the presynaptic active zone (Neher, 1998; Zhai and Bellen, 2004; Atwood, 2006). Although the spatial proximity of VGCCs and exocytic vesicles undergoing fusion with the plasma membrane is well documented, the detailed molecular mechanisms involved in the spatial and temporal coupling of exocytosis and VGCC activation and inactivation remain to be elucidated.

VGCCs are composed of an ion pore–forming $Ca_v\alpha1$ subunit associated with several auxiliary subunits ($Ca_v\beta$, $Ca_v\alpha2\delta$, and $Ca_v\gamma$; Arikkath and Campbell, 2003). Among the $Ca_v\alpha1$ subunits, the P/Q-type $Ca_v2.1$ and the N-type $Ca_v2.2$ define the main channel subtypes important for presynaptic neurotransmitter release (Spafford and Zamponi, 2003; Evans and Zamponi, 2006), and the L-type $Ca_v1.2$ subtype triggers Ca^{2+}-dependent secretion in neuroendocrine cells (Catterall, 2000). Four $Ca_v\beta$ subunit isoforms

Correspondence to Walter Hunziker: hunziker@imcb.a-star.edu.sg; or Thomas Launey: Thomas.launey@riken.jp

Abbreviations used in this paper: Ab, antibody; ABP, AID-binding pocket; AID, α1 interaction domain; BARP, β-anchoring and -regulatory protein; BDNF, brain-derived neurotrophic factor; GFAP, glial fibrillary acidic protein; hGH, human growth hormone; PSS, physiological salt solution; VGCC, voltage-gated calcium channel; WB, Western blot; WT, wild type.

Supplemental Material can be found at:
http://jcb.rupress.org/content/suppl/2014/04/17/jcb.201304101.DC1.html

The Rockefeller University Press $30.00
J. Cell Biol. Vol. 205 No. 2 233–249
www.jcb.org/cgi/doi/10.1083/jcb.201304101

Published April 21, 2014

($Ca_v\beta1$, $Ca_v\beta2$, $Ca_v\beta3$, and $Ca_v\beta4$) show distinct tissue and subcellular distributions (Dolphin, 2003; Buraei and Yang, 2010). $Ca_v\beta$ subunits interact with the 18-aa $\alpha1$ interaction domain (AID) of the cytoplasmic linker between internal repeats I and II of the pore-forming α_1 subunit (Pragnell et al., 1994; Chen et al., 2004; Opatowsky et al., 2004; Van Petegem et al., 2004). $Ca_v\beta$ subunits enhance VGCC channel activity (Mori et al., 1991; Chien et al., 1995; Josephson and Varadi, 1996; Kamp et al., 1996; Brice et al., 1997; Jones et al., 1998; Colecraft et al., 2002), not only by facilitating cell surface transport of VGCCs and by preventing ER-associated protein degradation (Altier et al., 2011) but also by modulating their gating properties (Buraei and Yang, 2010).

VGCCs interact via the $Ca_v\alpha1$ subunit with several pre- and postsynaptic proteins, including SNAP-25, synaptotagmin, syntaxin, Mint, and calcium/calmodulin-dependent serine protein kinase (Sheng et al., 1994; Bezprozvanny et al., 1995; Zhong et al., 1999; Maximov and Bezprozvanny, 2002; Spafford and Zamponi, 2003; Nishimune et al., 2004; Kang et al., 2006). The interaction and clustering of VGCCs with components of the secretory vesicle docking and fusion machinery by multiprotein adaptors highlights the importance of the spatial and temporal coordination of Ca^{2+} entry and neurosecretion (Yang and Berggren, 2006). The $Ca_v\beta$ subunits also interact with regulatory proteins that inhibit (e.g., RGK proteins, calcium, heterotrimeric G proteins, opioid receptor–like receptor 1, and several synaptic proteins) or facilitate VGCC activity (e.g., Rim1) or both (e.g., calmodulin; Herlitze et al., 1996; Ikeda, 1996; Lee et al., 1999; Béguin et al., 2001, 2005a,b, 2006, 2007; Beedle et al., 2004; Chen et al., 2005; Finlin et al., 2005; Evans and Zamponi, 2006; Jarvis and Zamponi, 2007; Kiyonaka et al., 2007; Buraei and Yang, 2010; Flynn and Zamponi, 2010; Yang et al., 2010).

Here, we describe a previously uncharacterized protein, which we term the VGCC–β-anchoring and -regulatory protein (BARP), and characterize its role in the regulation of VGCC activity and Ca^{2+}-regulated exocytosis. BARP is highly expressed in several specific neuronal populations and neuropeptide secretory cells, plays a role in the recruitment of $Ca_v\beta$ subunits to the plasma membrane, and negatively regulates VGCCs by interfering with the association of the $Ca_v\beta$ subunit with the $Ca_v\alpha1$ subunit. We hypothesize that BARP serves as an adaptor protein that modulates $Ca_v\beta$ subunit localization and their association with $Ca_v\alpha1$ subunits to regulate VGCC activity.

Results

Identification, tissue-specific expression, and membrane topology of BARP

BARP was identified in a yeast two-hybrid screen of a mouse insulin-secreting MIN6 cell cDNA library using $Ca_v\beta3$ as bait. BARP is encoded by an open reading frame of unknown function, C19orf26, which, based on its chromosomal location, has also been referred to as Dos (downstream of Stk11 kinase; Gerhard et al., 2004). Sequence analysis of EST clones and cDNA cloned from libraries revealed a ~3-kb transcript, coding for a 698-aa protein. BARP contains no known functional domains except for a single putative transmembrane domain and a putative N-glycosylation site (Figs. 1 A and S1 A). High BARP mRNA levels were found in brain, pancreatic islets, and neuroendocrine cell lines (MIN6 and PC12), with undetectable or weak expression in other tissues (Fig. 1 B).

The presence of BARP protein was confirmed in brain and PC12 cells using a polyclonal (72) and two affinity-purified mAbs (12B1 and 8B2) raised against different regions of the protein (Fig. 1 C). Specificity of the different antibody (Ab) was validated by the lack of staining in untransfected cells (Fig. S1 B) or after preabsorbing the Ab on a GST-BARP fusion protein (Figs. S1 C and S2 B) and by the absence of reactivity in pancreas-specific BARP knockout mice (Fig. S2 C). In COS-1 cells transfected with a Myc-tagged BARP cDNA, the labeling of the three Abs predominantly colocalized with that of the anti-Myc Ab (Fig. S1 B), but the BARP Ab did not colocalize with a Myc-tagged β-galactoside used as a negative control.

The predicted initiation methionine for BARP (M1; Fig. S1 A) is in accordance with the high quality annotation of the protein coding regions of the mouse and human genome by the Consensus Coding Sequence Project (Pruitt et al., 2009). This is the first conserved Met and the site where the high degree of amino acid identity among BARPs from different species starts (Fig. S1 D). In agreement with M1 being the initiation methionine, expression in COS-1 cells of mutants lacking either M7 or M80, the only two other conserved putative translation initiation sites in BARP, showed the same electrophoretic mobility as wild-type (WT) BARP, consistent with initiation of translation from M1 (Fig. S1 D). In contrast, the mobility of the M1A mutant was detectably faster than WT BARP, presumably because in the absence of M1, initiation can occur from M7. A truncated translation product was also obtained from the M1A/M7A mutant, presumably as a result of translation from M80 because only mutation of all three conserved methionine residues abolished translation. Thus, although M1, M7, and M80 can act as independent initiation sites, in the full-length cDNA, the codon for M1 serves as the main site for the initiation of translation.

BARP overexpressed in COS-1 or human embryonic kidney–derived tsA201 cells migrated as a doublet of higher molecular mass as compared with the in vitro translated BARP (Fig. 1 D), suggestive of posttranslational modifications. In PC12 cells, the upper band was more prominent. Tunicamycin led to a reduction of the apparent molecular mass for WT BARP but not for a mutant lacking the putative N-glycosylation site (^{25}N-X-S/T), consistent with the presence of N-linked glycosylation (Fig. 1 E). For better resolution of the different bands by SDS-PAGE, a C-terminal truncation of BARP (C-tr145, consisting of aa 1–145) was analyzed. After tunicamycin, PNGase F, or Endoglycosidase H treatment, the truncated form of BARP co-migrated with the truncated form lacking the N-glycosylation site (Fig. S1 E), confirming the presence of this glycosylation. After these treatments, however, BARP still migrated as a doublet, indicating the existence of additional unknown posttranslational modifications or internal initiation of translation.

The presence of N-terminal carbohydrate chains suggested that BARP is a type I membrane protein, with the N terminus located on the extracellular side. This topology was validated by cell surface labeling experiments, in which N- or C-terminally Myc-tagged BARP was expressed in COS-1 cells and the cells

Published April 21, 2014

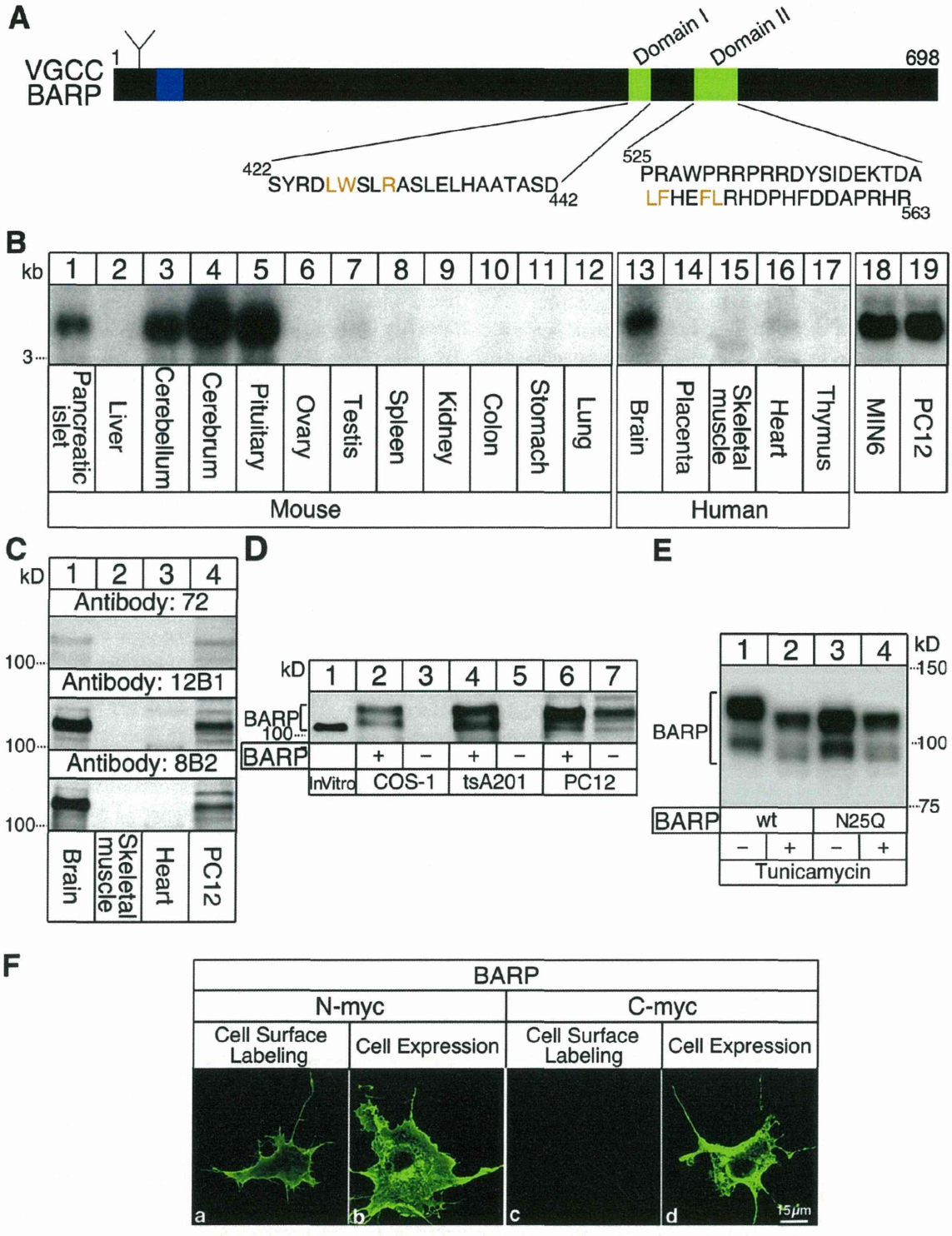

Figure 1. **Characterization of BARP.** (A) Structural and functional domains. The N-glycosylation site (Y), transmembrane region (blue), and the $Ca_v\beta$-interacting domain I and II (green) are depicted. Amino acid sequences of domain I and II, with residues crucial for interaction with $Ca_v\beta$ are in orange. (B) Northern blot analysis. BARP mRNA expression was analyzed in the indicated mouse and human tissues and cell lines. The samples were run on three separate gels, as shown. (C) WB analysis. Endogenous BARP protein was detected in brain and PC12 cells by WB using a rabbit polyclonal Ab (72) or two mouse mAb (12B1 and 8B2) raised against different regions of the protein. (D) Comparison of in vitro synthesized and cell-expressed BARP protein. BARP obtained by in vitro translation or from transfected COS-1, tsA201, or PC12 cells was analyzed by SDS-PAGE and WB (mAb 12B1). (E) BARP is N-glycosylated on Asn25. COS-1 cells expressing WT BARP or a BARP mutant lacking the putative N-glycosylation site (N25Q) were treated with tunicamycin to inhibit N-glycosylation. Cell lysates were analyzed by Tris/acetate-PAGE WB (Ab 72). (F) Membrane topology of BARP. Nonpermeabilized (cell surface labeling) or permeabilized (cell expression) are depicted. COS-1 cells expressing N- or C-Myc BARP were stained with an Ab to Myc and visualized by immunofluorescence microscopy. In nonpermeabilized cells (a and c), only the N-terminally tagged BARP was detected.

Published April 21, 2014

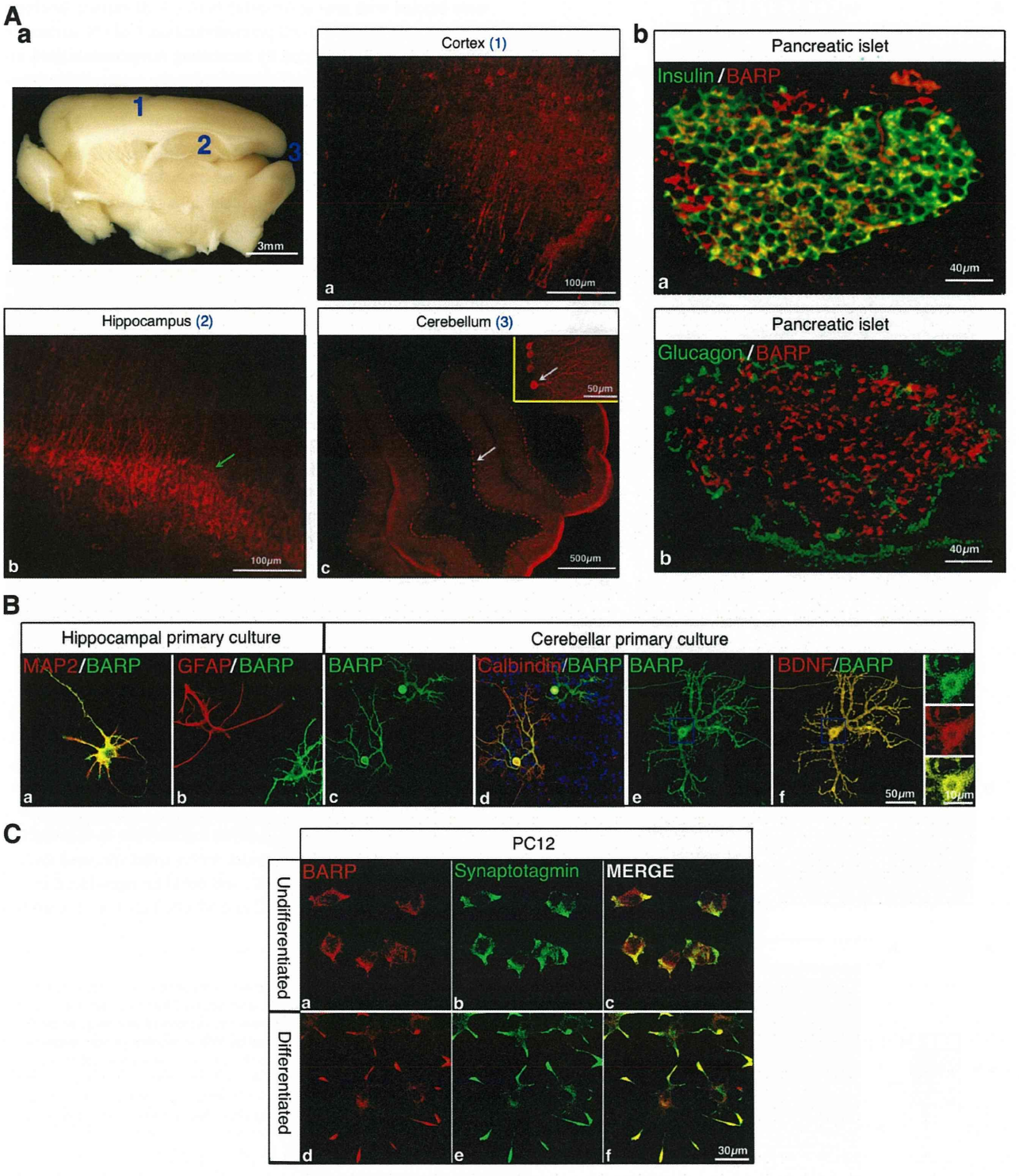

Figure 2. **Neuronal expression of BARP.** (A) Expression of BARP in brain (a) and pancreatic islets (b). Sections of cortex (1), hippocampus (2), and cerebellum (3) stained for BARP (mAb 12B1) and analyzed by immunofluorescence microscopy. BARP is detected in cell bodies and the dendritic extensions of Purkinje (white arrows) and pyramidal (green arrow) cells. In pancreatic islets, BARP is expressed in insulin-positive β cells but absent from α cells labeled for glucagon. The inset shows a higher magnification of the Purkinje cell layer. (B) Neuronal expression of BARP. Primary cells isolated from hippocampus or cerebellum were costained with mAb 12B1 to BARP and Ab to the neuronal marker MAP2 (a), the glial marker GFAP (b), the Purkinje marker calbindin (d), or the dense core vesicle protein BDNF (f). The insets show a higher magnification of the vesicular staining in the soma. Nuclei were stained with Hoechst (blue). (C) Colocalization of BARP with synaptotagmin in PC12 cells. Control or NGF-differentiated PC12 cells were costained with Ab to the regulated secretory vesicle marker synaptotagmin and BARP (Ab 72) and analyzed by confocal microscopy.

Published April 21, 2014

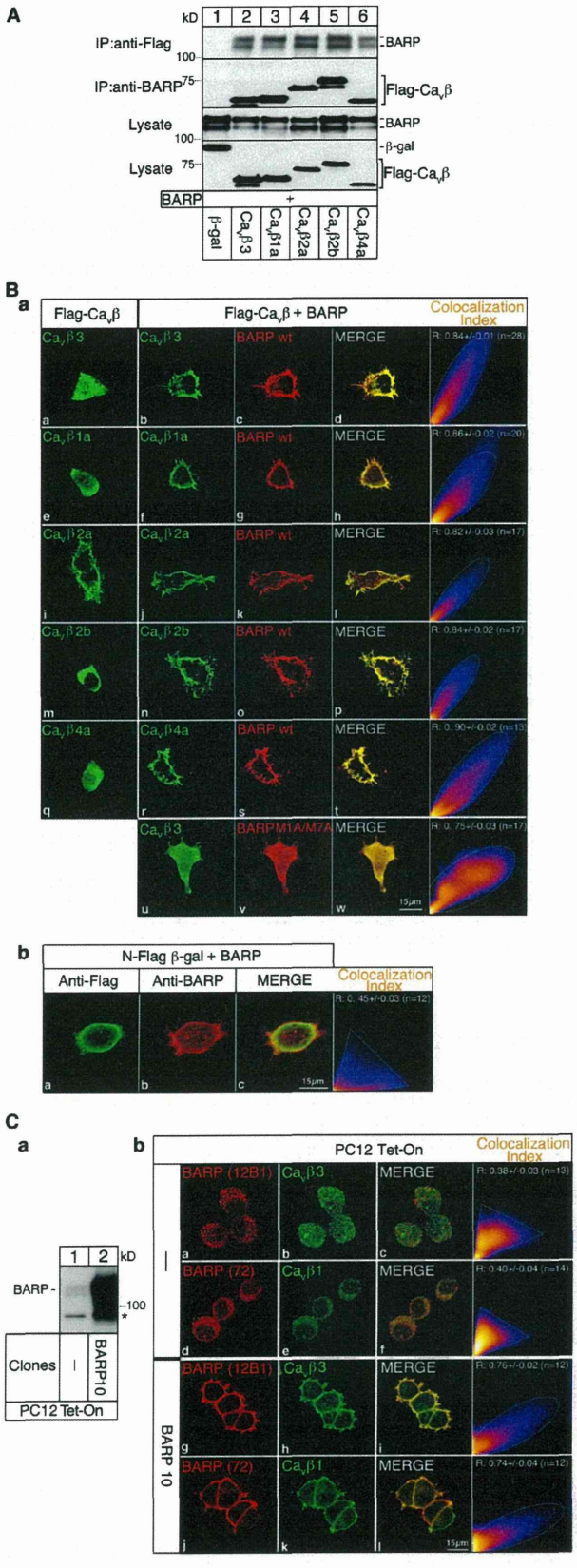

Figure 3. **BARP binds and localizes $Ca_v\beta$ subunits to the plasma membrane.** (A) Coimmunoprecipitation of $Ca_v\beta$ and BARP. COS-1 cells were cotransfected with cDNAs for BARP and the different Flag-tagged $Ca_v\beta$ subunit or, as a control, Flag–β-galactosidase (β-gal). Flag-tagged proteins were immunoprecipitated (IP), and bound BARP was detected by WB (Ab 72). The association was confirmed by reciprocal immunoprecipitation. Aliquots of cell lysates were analyzed by WB to monitor protein expression. (B) BARP localizes $Ca_v\beta$ subunits to the plasma membrane. (a) PC12 cells were transfected with cDNAs for the different Flag-$Ca_v\beta$ subunits, either alone or with a Myc-BARP cDNA. Cells were analyzed by immunofluorescence microscopy using Ab to Flag and Myc to detect the $Ca_v\beta$ subunits and BARP, respectively. Colocalization index is shown in the rightmost images. (b) Costaining of PC12 cells cotransfected with cDNAs for N-Flag–β-galactosidase, and Myc-BARP cDNA served as a negative control. (C) Constitutive overexpression of BARP relocates endogenous $Ca_v\beta$ subunits. (a) Protein expression. WB analysis of lysates from control PC12 Tet-On cells or cells constitutively expressing BARP. The asterisk indicates a nonspecific protein band. (b) Localization of endogenous $Ca_v\beta$ subunits to the plasma membrane upon BARP expression. Endogenous $Ca_v\beta$ subunits and endogenous (a–f) or stably overexpressed BARP (g–l) in PC12 Tet-On cell lines were detected by immunofluorescence microscopy. Colocalization index is shown in the rightmost images. The dotted lines delimit the cloud shape of the colocalization index. Note that imaging of endogenous BARP required a 10× longer exposure to obtain a comparable intensity to overexpressed BARP.

were labeled with antitag Ab either before (cell surface labeling) or after (cell expression) cell permeabilization. Only N-terminally tagged BARP was detected by incubating nonpermeabilized intact cells with Ab to Myc, thus confirming the extracellular exposure of the N terminus (Fig. 1 F).

Neuronal and pancreatic expression and subcellular localization of BARP

Immunolabeling of mouse tissue sections revealed BARP protein in the cortex, cerebellum, and hippocampus of the brain (Fig. 2 A, a) and in pancreatic islets (Figs. 2 A, b; and S2 C), consistent with the Northern blot analysis (Fig. 1 B). During mouse development, BARP expression in the brain peaked between embryonic day 18 (E18) and postnatal day 7 (P7; Fig. S2 A). In the cortex and hippocampus, BARP was detected in pyramidal cell bodies and dendrites. In the cerebellum, BARP was exclusively expressed in Purkinje cells, uniformly in soma and the main dendritic shaft and as a patchy staining along the distal dendrites (Figs. 2 A, a; and S2 B). Costaining of cultured primary cells isolated from hippocampus and cerebellum with BARP and neuronal (MAP2 and calbindin) or glial (glial fibrillary acidic protein [GFAP]) markers confirmed the neuron-specific expression of BARP (Fig. 2 B). In cerebellar primary cells, BARP was present in calbindin-positive Purkinje cells, where it localized to the cell soma, the dendritic shaft, and along the axon, including the presynaptic button, and colocalized with the dense core vesicle marker brain-derived neurotrophic factor (BDNF).

In PC12 cells, BARP partially colocalized with the Ca^{2+}-dependent secretory vesicle markers synaptotagmin I and, upon NGF-induced differentiation, localized to the growth cone (Fig. 2 C). In contrast to the more prominent vesicular staining of endogenous BARP in PC12 cells (Fig. 3 C, b), BARP overexpressed in PC12 or other cell lines was enriched at the plasma membrane (Fig. S2, D and F). Such a difference in distribution was also reported for endogenous versus overexpressed synaptotagmin I (Vega and Hsu, 2001) and could be reproduced in our PC12 cells (compare Figs. 2 C and S2 D). This was interpreted

Published April 21, 2014

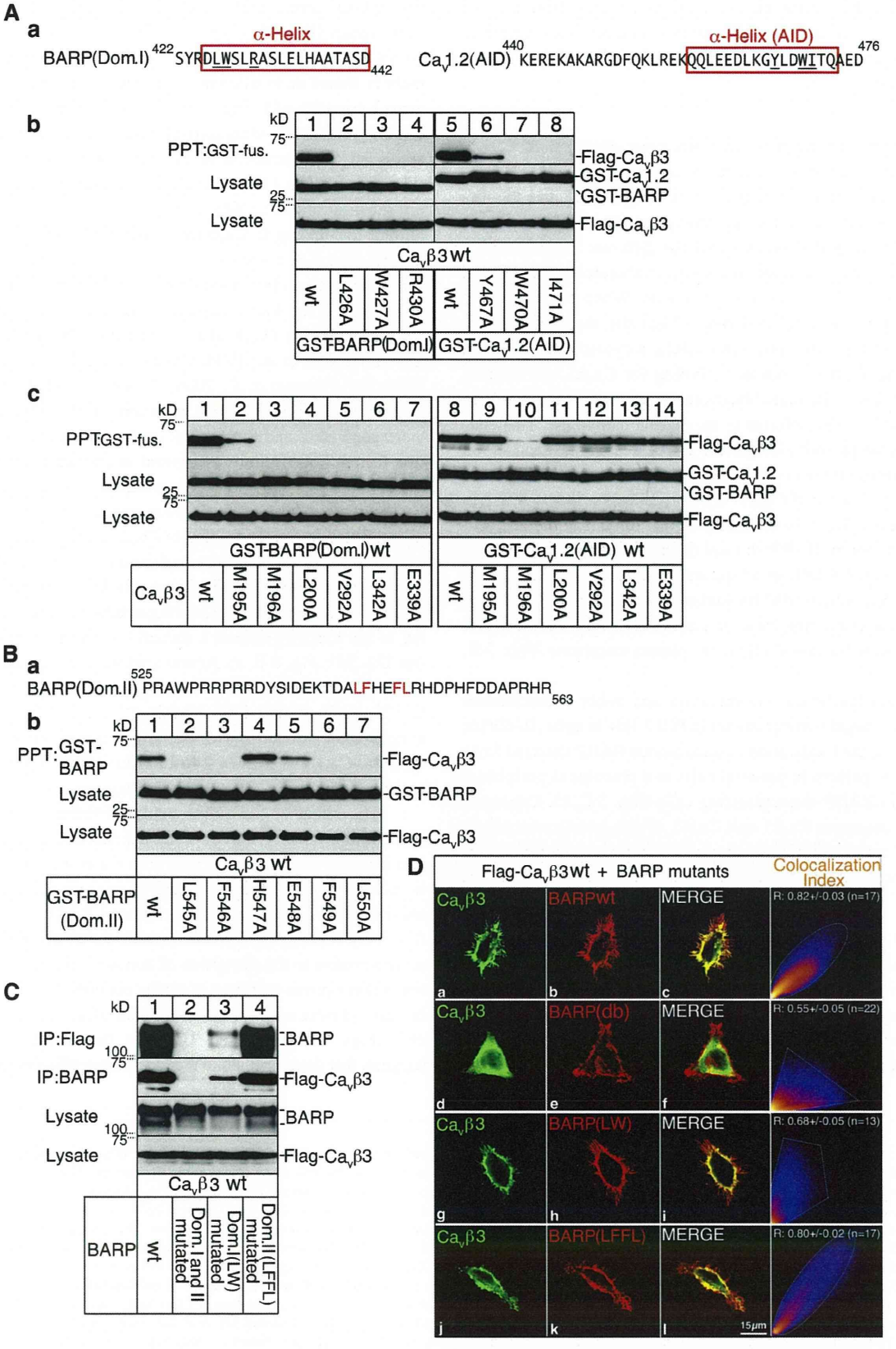

Figure 4. **BARP associates with $Ca_v\beta$ subunits via domain I and domain II.** (A) Identification of BARP domain I (Dom.I) as a $Ca_v\beta$-interacting domain. (a) Amino acid sequence of domain I and AID. The predicated (BARP) or known ($Ca_v1.2$ AID) α helix and amino acids important for $Ca_v\beta$ binding (underlined) are shown. (b) Identification of amino acids in domain I important for binding to the $Ca_v\beta$. COS-1 cells expressing Flag-$Ca_v\beta3$ and WT or mutated